



## Numerical Simulation of Turbulent Gas Flow in a Solid Rocket Motor Nozzle

A. Balabel\*, A.M. Hegab\*\*, S. Wilson\*, M. Nasr\*, S. El-Behery\*

**Abstract:** The purpose of the present study is to demonstrate the numerical accuracy of different turbulent models that can predict the physical properties and physical phenomena of turbulent gas flow in a solid rocket nozzle. The nozzle is assumed to have a convergent-divergent geometry with impermeable and adiabatic walls. The entrance flow is subsonic with known properties, while the properties at the exit plane for the supersonic flow are determined by extending the computational domain outside the nozzle. The time-dependent, compressible Navier-Stokes equations with turbulent effects are solved using a 2-D finite volume Navier Stokes solver based on the SIMPLE algorithm. Different turbulence models are applied and assessed by comparing the obtained results of the static wall pressure and the shock position with the available experimental data. The dimensionless shear stress at the nozzle wall and the separation point are also predicted. Among the turbulence models adopted, the shear-stress transport (SST)  $k-\omega$  model gave the best overall agreement with the experimental measurements. The results indicate that the shock position moves downstream by increasing the nozzle pressure ratio to a certain maximum value corresponding to the prescribed geometry, at which the shock did not change its location nearby the nozzle exit. In general, the numerical procedure adopted in the present paper shows good capability in predicting the physical phenomena encountered.

Keywords: Numerical simulation, Compressible flow, turbulence Models, convergent-divergent nozzle

### 1 Introduction

The numerical solution of turbulent compressible flows in nozzles is a challenge problem in fluid dynamics applications. Recently, an extension studies have been devoted to understand the fluid dynamics phenomena in solid rocket motor nozzles. The increased attention is due to a host of technological applications. One example of an important problem is the exhaust gas from jet engines and solid propellant rocket motor. The internal nozzle flow development of a solid rocket plays an essential role both in nozzle design and performance. In particular, the mean velocity field, the axial pressure distribution and the turbulence characteristics have a strong and direct impact on many physical processes occurring within the nozzle.

---

\* Mechanical Power Engineering Department, Faculty of Engineering, Menoufiya University, Shebin El-Kom, EGYPT

\*\* Mechanical Power Engineering Department, Faculty of Engineering, Menoufiya University, Shebin El-Kom, EGYPT, Corresponding author: [hegab2002us@yahoo.com](mailto:hegab2002us@yahoo.com), Tel. 012-7858517

The majority of the previous studies on the solid rocket motors have involved the investigations of a nozzleless rocket motor to study the applicability of turbulence models and a DNS analysis to this type of flows [[1]]. The flow behavior inside the combustion chamber of a solid rocket plays a key role in both motor design and operation. However, in real solid rocket motor, both the chamber and nozzle geometries have significant effects on the overall performance. The combustion chamber-nozzle configuration can affect the relationship between the propellant burning rate transients and the co-existing acoustic waves [2,3].

A full treatment of such problems would include the modeling and resolution of complex physical and chemical phenomena which occurs during the solid propellant combustion process. These models are characterized by extremely diverse length and time scales, complex interfaces, reactive, turbulent, and multiphase flows. These complexities are still a big challenge to perform the whole system simulation. Therefore, many investigations have been directed to modeling, design and testing of solid rocket nozzles aiming to a better nozzle performance, e.g. [4,5]. The main conclusion of such investigations was the important effects resulting from the addition of a divergent section to the convergent nozzle. The divergent section provided further expansion of the flow to supersonic conditions at the nozzle exit; resulted in an increase in momentum thrust. However the Convergent-Divergent (CD) nozzles often incorporate variable geometry to maintain high performance over a wide range of operating conditions. For best efficiency, the required nozzle area ratios are much higher at supersonic flows than subsonic flows. All propulsion systems with CD nozzles may experience a development of diamond pattern occurs downstream from the nozzle which results from expansion and compression waves according to under- or over-predicted regime. However, propulsion systems which have the advantage of variable geometry nozzles operate closer to design conditions than those with fixed geometry nozzles

Generally, the propulsive force provided by a rocket nozzle is a function of many parameters such as exit to throat area ratio, type of fuel and oxidizer used and the real chamber pressure to the outside one. In addition, a reliable separation model is needed for accurate prediction of the side-loads experienced during startup and shutdown of the engine. A better understanding of flow separation phenomena in over-expanded rocket nozzle could lead to better prevention or even control of flow separation. Moreover, the advancement of exhaust nozzle technology has essential and great effect on the development of gas turbine engines and solid rocket motors.

To understand the previous research efforts on these topics, several research papers can be found in the literature. The majority of these investigations is focused on the formation and transportation of shock wave inside a convergent-divergent nozzle and its contribution to the instability of the separation shear layers. When a supersonic nozzle is operated at pressure ratios well below its design point, a shock forms inside the nozzle and the flow downstream of the shock separates from the nozzle wall. Numerous past studies have thoroughly investigated supersonic flow separation in over-expanded rocket nozzles [6-12]. A paramount issue is the prediction of the separation location and the separation pressure ratio is defined as the ratio of the pressure just ahead of separation to the ambient pressure.

Although there is a large amount of studies concerning the flow separation in CD nozzles over a wide range of nozzle pressure ratio (NPRs), the detailed investigation on separation flow mechanism is less matured. It seems that this phenomenon is very basic, even though it remains poorly understood. Most of available publications are concentrated on prediction of separation location. Moreover, several researches have investigated the shock structure in

over-expanded CD nozzles. In both cases, a high degree of accuracy is required in order to predict the thrust coefficient adequately. The importance of the thrust coefficient in avoiding booms in takeoff can be seen in [13].

The computational studies of the flow field through CD nozzles are based on the solution of the time-dependent; Reynolds averaged Navier-Stokes (RANS) equations and the implementation of an appropriate turbulence model for closure of the RANS equations. The governing equations are solved in generalized coordinates and in conservative form. The previous numerical studies have assessed the accuracy of the turbulence model for predicting the flow field and the thrust performance accurately. In general, the turbulence model performance in the flow regions dominated by strong pressure gradients and complex secondary flows can be considered as the most likely culprit for the discrepancies observed between the numerical simulations and the experimental measurements.

Several turbulence models can be used for the computational study ranging from an algebraic to linear and nonlinear two-equation turbulence models. An algebraic model is accurate for simple viscous flows because the turbulent viscosity is determined by a local function. The two-equation turbulence model with second-order closure is used to model more complex viscous flow features such as shear layer and regions of separated flow. The implementation of non-linear eddy viscosity turbulence models is another important topic in the recent modeling of turbulent flow. This approach is based on the nonlinear extension of the linear stress-strain relation which base on Boussinesq-hypothesis. Nonlinear constitutive equations have been proposed to overcome the limitations of linear eddy viscosity models in describing complex turbulent flow. The non-linear turbulence models have proved their capability to predict the reattaching turbulent shear flow in asymmetric divergent channel in our previous research [[14]]. However, numerical stability is often problematic and often small time step is required for stability. The same problem can be seen by using the Reynolds-stress transport models in complex flows.

This state of affairs leaves methods that are rely on RANS equations as the most promising alternative for practical engineering computations. Recently, RANS modeling is used to predict most of complex viscous flows feature encountered in engineering applications such as shear layers and regions of separated flow in conjunction with near wall function or damping function to adjust the turbulent viscosity near the solid walls. Even in two-phase flows, the RANS modeling can be used in a wide range [[15]]. Although, a complete agreement with experiments is not achieved, these models succeeded in resolving complex features of both the mean flow and turbulence field. Our research group has tested, in parallel research, five different turbulence models for predicting turbulence in porous channel with constant mass injection [16]. The obtained results showed that the two-equation  $k-\varepsilon$  turbulence model can be extended and used in such complex flows.

Recently, five turbulence models have been assessed in terms of their effects on the agreement between the experimental centerline pressure distribution and the 2D computational results at over-expanded conditions [17]. The turbulence models considered are the algebraic models of Baldwin-Lomax, RNG, the one equation model of Baldwin-Barth and the two-equation  $k-\varepsilon$  and  $k-\omega$  models of Chien and Wilcox. Their results indicated that both the shock location and pressure level behind the shock are strongly affected by the turbulence model, where agreement with experimental data has been obtained only up to the point of shock and then varied significantly in the predicted shock location and pressure level behind the shock. In the 3D simulations, the computed results are very sensitive to the turbulence

models and the two-equation models could predict good results. In addition, they demonstrated that the interactions created through external flow entrainment, and their effects on surface pressure distribution, might not be adequately simulated if only the nozzle interior domain is considered.

The two-equation  $k-\omega$  turbulence model in conservation law form and general curvilinear coordinate in [18] is used to predict the surface pressure distribution and internal thrust coefficient of a 2DCD nozzle. In comparison with the results obtained using Spalart-Allmaras turbulence model, they confirmed the importance of the turbulence model in producing realistically or unrealistically numerical results [19].

Although of the wide application of several turbulence models in a variety of flow fields, it is yet remains a widely debated subject. Even though some experiments and analysis have shown that the motion of the shock wave can be affected by turbulent fluctuations in the attached boundary layer in upstream direction [20], it would seem that in general, the initial perturbations comes from fluctuation in the downstream separated flow [21]. Through the measurements of the wall pressure spectra near the recirculation regions, two spectral lower and higher frequency bumps have been observed [22]. This has been attributed to the finite length of the larger and smaller recirculation zones respectively.

Because the motivation behind our present investigation is to demonstrate a numerical method that can predict the physical phenomena of turbulent gas flow in a solid rocket nozzle with an appropriate turbulence model, our primary focus is not the source of the shock unsteadiness but rather the impact of the turbulence model adopted on the shock position and movement on the flow downstream and its contribution to the instability of the separation shear layer. The general prediction method for heat and mass transfer proposed by [23] was used to obtain the numerical solution of the two-dimensional compressible Reynolds averaged Navier-Stokes (RANS) equations. This numerical method is based on the SIMPLE algorithm stands for Semi Implicit Method for Pressure Linked Equations [Patankar, 1980]. Several turbulence models; namely the standard  $k-\varepsilon$  (STD) model [24], the extended  $k-\varepsilon$  (ETD) model [[25]], the  $k-\varepsilon-v^2-f$  ( $v^2-f$ ) model [26] and shear-stress transport (SST)  $k-\omega$  model [27], are used in the present numerical simulation in predicting the internal nozzle flow over a wide rang of nozzle pressure ratios. The comparison with the available experimental data is used to asses the accuracy of the turbulence model adopted.

## 2 Computational Code and Procedure

The finite volume solver, proposed by [[23]], is used to obtain the numerical solution of the two-dimensional compressible Reynolds averaged Navier-Stokes (RANS) equations by using a number of turbulence models for closure of the RANS equations. The governing equations are solved in general curvilinear coordinates and in conservative form. The discretised equations, along with the initial condition and boundary conditions, were solved using the segregated solution method. The pressure velocity coupling was obtained by SIMPLE algorithm. Using the segregated solver, the conservation of mass and momentum were solved sequentially and a pressure-correction equation was used to ensure the conservation of momentum and the conservation of mass (continuity equation). Several turbulence models, i.e. the standard  $k-\varepsilon$  model, the extended  $k-\varepsilon$  model, shear-stress transport  $k-\omega$  model, and the  $v^2-f$  model are tested. The extended  $k-\varepsilon$  model differs from the standard  $k-\varepsilon$  model in its constant and it has an additional source term in the  $\varepsilon$  equation. This model was implemented in the code by adjusting the standard  $k-\varepsilon$  model constants and by defining the additional

source term. For more details about the numerical procedure, one can refer to our previous paper [[14]].

### 2-1 Near-wall modeling

In the region near the wall, the gradient of quantities is considerably high and requires fine grids close to the wall to capture the changes of quantities. For complex flows where separation flow and reattachment occur, the conventional logarithmic wall-function proposed by Launder and Spalding [[28]] becomes less reliable. The non-equilibrium wall-function proposed by Kim and Choudhury [[29]] is proven to give better predictions since it accounts the effects of pressure gradient and departure from equilibrium. For the standard k- $\epsilon$  model and the extended k- $\epsilon$  model, the non-equilibrium wall-function is applied to the wall-adjacent cells, while for  $v^2$ - $f$  model models the near-wall turbulence is treated without the use of exponential damping or wall functions. For the SST k- $\omega$  models, if the *transitional flows option* is enabled in the viscous model panel, low-Reynolds-number variants will be used, and, in that case the near-wall grids have to be very fine to obtain the better results for the near wall modeling. If *transitional flows option* is not active as in the present study, the near wall grids follow a rule of the wall function.

The use of a wall function in a computational flow solver allows fewer points to be placed near the walls where these points are typically placed to  $Y^+ = 1$  for a wall integrated grid. In the present study  $Y^+$  changed from 0.8 to 1.1 depending on the nozzle pressure ratio and on the selected turbulence model.

### 2-2 The governing equations

The governing equations consist of the continuity equation and the Reynolds-averaged governing equations for steady compressible turbulent flow coupled with the equation of state,  $p = \rho RT$ . The system of the governing equations can be described as follows:

#### The continuity equation:

$$\frac{\partial}{\partial x_i}(\rho u_i) = 0 \quad (1)$$

#### RANS equations:

$$\frac{\partial}{\partial x_j}(\rho u_i u_j) = -\frac{\partial p}{\partial x_i} + \frac{\partial}{\partial x_j} \left[ \mu \left( \frac{\partial u_i}{\partial x_j} + \frac{\partial u_j}{\partial x_i} - \frac{2}{3} \delta_{ij} \frac{\partial u_l}{\partial x_l} \right) \right] + \frac{\partial}{\partial x_j} (-\overline{\rho u'_i u'_j}) \quad (2)$$

#### Energy equations:

$$\frac{\partial}{\partial t}(\rho E) + \frac{\partial}{\partial x_i} [u_i(\rho E + p)] = \frac{\partial}{\partial x_j} \left( \left( k + \frac{C_p \mu_t}{0.85} \right) \frac{\partial T}{\partial x_j} + u_i (-\overline{\rho u'_i u'_j}) \right) \quad (3)$$

where  $u$  denotes mean quantities and the  $u'$  fluctuating or turbulence quantities,  $\rho$  is density,  $p$  is pressure,  $\mu$  is viscosity. The additional fluctuating quantities known as the Reynolds

stresses, which must be modeled in order to close the system of equations. The apparent turbulent shearing stresses might be related to the rate of mean strain through an apparent scalar turbulent or "eddy" viscosity. For the general Reynolds stress tensor, the Boussinesq assumption gives:

$$-\overline{\rho u'_i u'_j} = \mu_t \left( \frac{\partial u_i}{\partial x_j} + \frac{\partial u_j}{\partial x_i} \right) - \frac{2}{3} (\rho k + \mu_t) \frac{\partial u_k}{\partial x_k} \delta_{ij} \quad (4)$$

where  $\delta_{ij}$  is the Kronecker delta function ( $\delta_{ij}=1$  if  $i=j$  and  $\delta_{ij}=0$  if  $i \neq j$ ),  $k$  is the turbulent kinetic energy and  $\mu_t$  is the turbulent viscosity.

### 2-3 Turbulence models

As mentioned above, turbulence modeling is required for closure of RANS equations. In the present paper, four turbulence models are tested and evaluated for the case considered; namely: the standard  $k-\varepsilon$  (STD) model [24], the extended  $k-\varepsilon$  (ETD) model [25], the  $k-\varepsilon-v^2-f$  ( $v^2-f$ ) model [26] and shear-stress transport (SST)  $k-\omega$  model [27]. The general transport equations for the adopted models are given below, while the different terms and coefficient of the turbulence models adopted are given in Table 1.

#### The $k$ - equation:

$$\frac{\partial}{\partial x_j} (\rho u_j k) = \frac{\partial}{\partial x_j} \left[ \left( \mu + \frac{\mu_t}{\sigma_k} \right) \frac{\partial k}{\partial x_j} \right] + \rho (P_k^* - \beta_1 \varepsilon - \beta_2 k \omega) \quad (5)$$

#### The $\varepsilon$ - equation:

$$\frac{\partial}{\partial x_j} (\rho u_j \varepsilon) = \frac{\partial}{\partial x_j} \left[ \left( \mu + \frac{\mu_t}{\sigma_\varepsilon} \right) \frac{\partial \varepsilon}{\partial x_j} \right] + \frac{\rho}{T} (C_{1\varepsilon} P_k - C_{2\varepsilon} \varepsilon + C_{3\varepsilon} \frac{P_k^2}{\varepsilon}) \quad (6)$$

#### The $v^2$ - equation:

$$\frac{\partial}{\partial x_j} (\rho u_j v^2) = \frac{\partial}{\partial x_j} \left[ \left( \mu + \frac{\mu_t}{\sigma_k} \right) \frac{\partial v^2}{\partial x_j} \right] + \rho (k f - v^2 \frac{k}{\varepsilon}) \quad (7)$$

#### The $f$ - equation:

$$L^2 \frac{\partial^2 f}{\partial x_j^2} - f = \frac{1}{T} \left[ (-4.6) \frac{v^2}{k} - \frac{0.8}{3} \right] - 0.3 \frac{P_k}{k} \quad (8)$$

**The  $\omega$ - equation:**

$$\frac{\partial}{\partial x_j} (\rho u_j \omega) = \frac{\partial}{\partial x_j} \left[ \left( \mu + \frac{\mu_t}{\sigma_\omega} \right) \frac{\partial \omega}{\partial x_j} \right] + \rho^2 \frac{\gamma_1}{\mu_t} P_k - \rho \beta_3 \omega^2 + F_{SST} \quad (9)$$

**Table 1 Coefficient for turbulence models**

	STD $k$ - $\varepsilon$ model	ETD $k$ - $\varepsilon$ model	$v^2$ - $f$ model	SST $k$ - $\omega$
$\beta_1$	1	1	1	0
$\beta_2$	0	0	0	0.09
$\beta_3$	0	0	0	0.0828
$\sigma_k$	1	0.75	1	1
$\sigma_\varepsilon$	1.3	1.15	1.3	0
$\sigma_\omega$	0	0	0	1.168
$P_k$	$2\nu_t S_{ij} S_{ij}$	$2\nu_t S_{ij} S_{ij}$	$2\nu_t S_{ij} S_{ij}$	$2\nu_t S_{ij} S_{ij}$
$S_{ij}$	$0.5(u_{i,xj} + u_{j,xi})$	$0.5(u_{i,xj} + u_{j,xi})$	$0.5(u_{i,xj} + u_{j,xi})$	$0.5(u_{i,xj} + u_{j,xi})$
$P_k^*$	$P_k$	$P_k$	$P_k$	$\text{Min}(P_k, 10\varepsilon)$
$C_{1\varepsilon}$	1.4	1.15	$1.4(1+0.05(k/\nu^2)^{0.5})$	0
$C_{2\varepsilon}$	1.92	1.9	1.9	0
$C_{3\varepsilon}$	0	0.25	0	0
T	$k/\varepsilon$	$k/\varepsilon$	$\text{Max}(k/\varepsilon, 6(\mu/\rho\varepsilon)^{0.5})$	0
$\mu_t$	$\rho C_\mu k^2/\varepsilon$	$\rho C_\mu k^2/\varepsilon$	$\rho C_\mu \nu^2 T$	$0.31\rho k/\text{Max}(0.31\omega, F_2(2 S_{ij} S_{ij})^{0.5})$
$C_\mu$	0.09	0.09	0.22	0
L	0	0	$0.23\text{Max}(k^{1.5}/\varepsilon, 70(\nu^{0.75}/\varepsilon^{0.25}))$	0
$F_2$	0	0	0	$\tanh(D_1)^2$
$D_1$	0	0	0	$((2k^{0.5}/0.09\omega y), 500\nu/\omega y^2)$
$\gamma_1$	0	0	0	0.4403
$F_{SST}$	0	0	0	$2.336(1-F_1)(1/\omega)(k_{,xi}\omega_{,xi})$
$F_1$	0	0	0	$\tanh(D_2)^4$
$D_2$	0	0	0	$\text{Min}(\text{Max}(D_1, 4.672\rho k/D_3 y^2)$
$D_3$	0	0	0	$\text{Max}(2.336\rho(1/\omega)(k_{,xi}\omega_{,xi}), 1.e^{-10})$

The effect of compressibility on turbulence models is known as "dilatation dissipation". The considering of compressibility effect enables the prediction of the observed decrease in spreading rate with increasing Mach number for compressible mixing and other free shear layers.

**2-4 Computational domain and computational grid**

A 2D computational domain with the assigned boundary conditions is shown in figure 1. A grid generation for the upper half of the nozzle with 260x100 grids and compression factor of 0.97 is shown on the right hand side in figure 1b. This grid was selected after a grid refinement study was conducted for nozzle pressure ratio of 2.412.

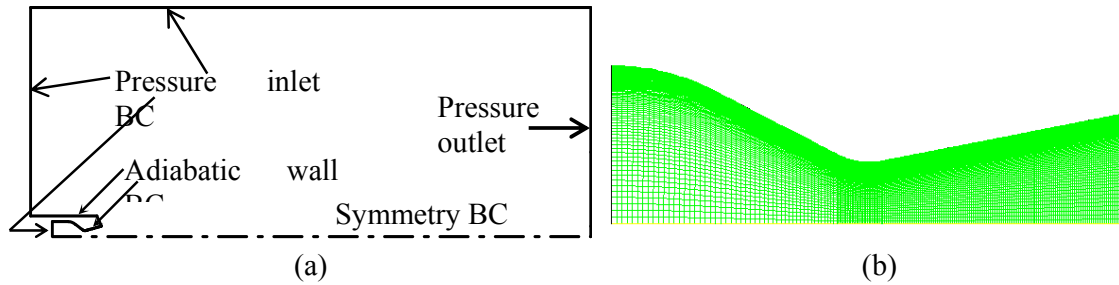


**Figure 1 (a) Computational domain and (b) computational grid**

### 2-5 Boundary conditions

The assigned boundary conditions, as prescribed in figure 1a are declared as follows. The Pressure outlet boundary conditions are specified on the right boundaries, which require the specification of a static (gauge) pressure at the outlet boundary when the flow is subsonic. Should the flow become locally supersonic, the specified pressure will no longer be used and the pressure will be extrapolated from the flow in the interior. All other flow quantities are extrapolated from the interior.

Ambient pressure and temperature conditions are considered as total conditions at the top and left external boundaries, while stagnation conditions are specified at the inlet to duct upstream of the nozzle. In addition, a static pressure was specified at the duct inlet to start the solution. Symmetry boundary conditions are applied at the symmetry plane, and no-slip conditions at the walls.

### 3 Validations

The validations of the turbulence models adopted in the present computational investigation are based on the comparison of the static pressure on the upper nozzle surface with the experimental measurements [30] at different Nozzle Pressure Ratio (NPR). The NPR is defined as the ration of the total (or stagnation) pressure at the nozzle inlet  $P_o$  and the ambient pressure  $P_a$ . The exhaust flow pattern is dependent on whether the flow is under-expanded for the design nozzle pressure ratio  $NPR_D > 1$  or over-expanded for  $NPR_D < 1$  [[18]]. Because of the external exhaust flow expansion has a free (ambient-exhaust) boundary, the nozzle performance characteristics is a function of NPR, Mach number  $M$  and the angle of attack. However, in the static (wind-off) investigation, the internal performance parameters depend on NPR only. Moreover, the flow pattern, shock structure, flow separation and shear layer detachment are strongly affected by the NPR.

In the present paper, a wide range of NPR is considered. Figure 2(a, b, c) shows the comparison between the computational results obtained using the four turbulence models presented earlier (cf. section 2) and the experimental measurements found in [30]. The static wall pressure is normalized using the stagnation pressure  $P_o$  and plotted against the non-dimensional streamwise location  $x/x_t$ , where  $x_t$  is the streamwise location at nozzle throat. The comparison is made for NPR=1.255, 3.014 and 5.423.

For low NPR=1.255, as shown in figure 2a, the pressure fields indicate a weak shock near the geometric throat and the internal flow downstream of the shock is over-expanded and appears to recover to the ambient pressure smoothly and in continuous manner. By comparing the

capability of the used turbulence models in predicting the shock formation and position, it is found that the numerical predictions using the SST turbulence model showed close agreement with the experimental measurements. In contrast, the ETD turbulence model illustrates over-predicted pressure distribution. This behavior is clearly seen in the recovery region while give nearly the same shock position. However, the STD and  $v^2-f$  turbulence models under-predicted the pressure distribution and give a different shock position in the downstream direction.

For medium NPR=3.014, shown in figure 2b, the shock position nearly approaches the nozzle exit and there was almost no pressure recovery downstream of the shock. This result indicates that the internal flow adjusted itself to the exit conditions by completely detaching past the shock. The SST turbulence model predicts the experimental measurements in good agreement, while the results of the ETD turbulence model could be accepted with some cautions. In contrast, the results of the STD and  $v^2-f$  turbulence models show large deviations from the experimental measurements especially downstream of the shock position.

By increasing the NPR to be about 5.423, as shown in figure 2c, the numerical results show that the nozzle is shock free. The pressure falls downstream the nozzle throat indicates that the internal flow is found to be independent of the NPR. By comparing the numerical results obtained from the four turbulence models, the SST turbulence model is nearly the more suitable model in predicting the experimental data and the pressure distribution. The ETD turbulence model gave also good agreement; however, this model shows a little increase in the wall pressure near the nozzle exit in order to match the prescribed boundary conditions. The success of the ETD turbulence model in this range of NPR may be referred to the shock free internal flow. However, the STD  $k-\varepsilon$  and  $v^2-f$  turbulence models still give over-predicted results in spite of the absence of shock inside the nozzle.

From the above comparison, it is found that numerical predictions using the SST transport turbulence model showed close agreement with the experimental results more than that given by the other turbulence models. The formulation of SST turbulence model in the gradual change from the standard  $k-\omega$  model in the inner region of the boundary layer to a high-Reynolds-number  $k-\varepsilon$  model in the outer part of the boundary layer enables it from capturing the shock wave boundary layer interaction accurately. In addition, the turbulent viscosity is modified to account for the transport effects of the principal turbulent shear stress. The other models are  $k-\varepsilon$ -based turbulence model; therefore, different degree of accuracy is obtained according to the modifications made. The ETD turbulence model proposed an extra time scale of the production range included in the dissipation rate equation. That pushes the model to perform quite well in the turbulent boundary layer flows. The STD  $k-\varepsilon$  and  $v^2-f$  turbulence models need further improvement to be suitable for the shock wave turbulent boundary layer interaction applications. As a result, the SST turbulence model is considered to be the base of the current turbulence model.

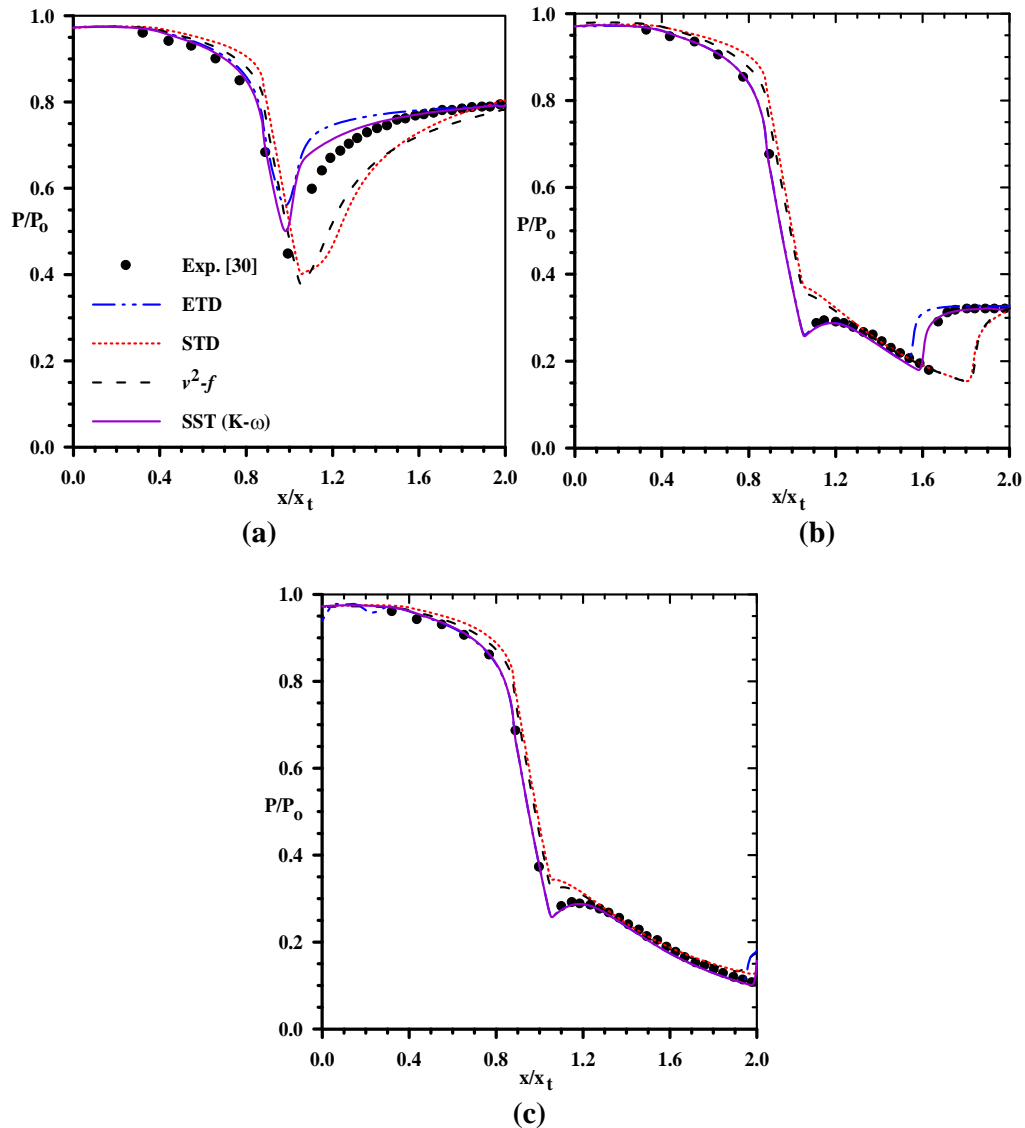


**Figure 2 Comparison of the present results with the experimental measurements [[30]] for the turbulence models adopted (a, NPR=1.255, b, NPR=3.014, c, NPR=5.423)**

## 4 Results and Discussion

The computed Mach number images for different NPRs 1.255, 2.412, 2.607, 3.014, 5.423 and 7.03 are plotted in Figure 3 (a, b, c, d, e, and f), respectively. These images describe briefly the principal separation phenomena in a symmetric nozzle. One can see clearly near the wall, the separation shock consists of incident and reflected oblique waves that merge into a Mach stem at the triple point. This is so-called lambda foot of the shock [31].

The present results show, for low NPR=1.255, a weak normal shock downstream of the nozzle throat with no lambda foot structure evident. However, the results show, for NPR=2.412, a nozzle shock with a pronounced lambda foot structure and fully detached separation layer extended from the leading lambda shock in downstream. The separation region formed downstream can be considered as consequence of the adverse pressure gradient through the shock, which forces the incoming boundary layer to separate. The oblique shock

structures are of the weak type resulting in low supersonic flow downstream while the flow immediately past the Mach stem is subsonic.

The same results are obtained for subsequent NPRs greater than 2.412, e.g. NPR=2.607, 3.014, as shown in figure 3(c, d). Moreover, the separation shear layers emerged as expansion fans and transmitted across the test section to the opposite shear layer where they reflected again as compression waves. This reflection continues downstream, resulting in a series of expansion and compression waves through the separation region.

By increasing the NPR, the lambda shock foot had grown significantly, such that the main shock and the trailing lambda foot were located behind the nozzle exit. The nozzle was shock free and the flow was over-expanding externally, as shown in figure 3(e, f) for NPR=5.423, and NPR=7.03.

The previous results indicate that the shock motion inside the nozzle and the separation point are affected by the NPR. Therefore, a wide range of NPRs has been simulated using the SST turbulence model. The predictions of the shock position as well as the separation point were plotted and compared with the experimental measurements [30], as shown in figure 4. The results indicate that by increasing the NPR, the shock position as well as the separation point move downstream. For the present given geometry, there is a maximum NPR (NPR $\approx$ 5) over which the shock did not change its location nearby the nozzle exit.

The dimensionless shear stress ( $\tau/\tau_{in}$ ) distribution for different NPRs is plotted in figure 5, where  $\tau_{in}$  is the shear stress at the nozzle inlet. For separated flow and low NPR, the results indicate that the flow did not attach the nozzle surface and the free shear layer started at the trailing lambda foot was completely detaching past the shock. As the separation point became nearly the effective nozzle exit, the lambda shock system adjusted to satisfy continuity of pressure and flow direction. This is indicated by a slight increase of the shear stress near the nozzle exit. These results can also be seen in the velocity vector graph, figure 6, for NPR=2.412, where a positive velocity distribution is obtained nearby the effective nozzle exit.

Figure 7, illustrates the computational shock schematic for NPR=2.412 compared with both the experimental measurement and the computational result of [30]. The present predicted shock height equals  $\approx 0.61$  inch. Its value is located between the experimental measurements and the numerical results of [30], but closer to the experimental data. That indicates the accuracy of the present numerical simulation performed.

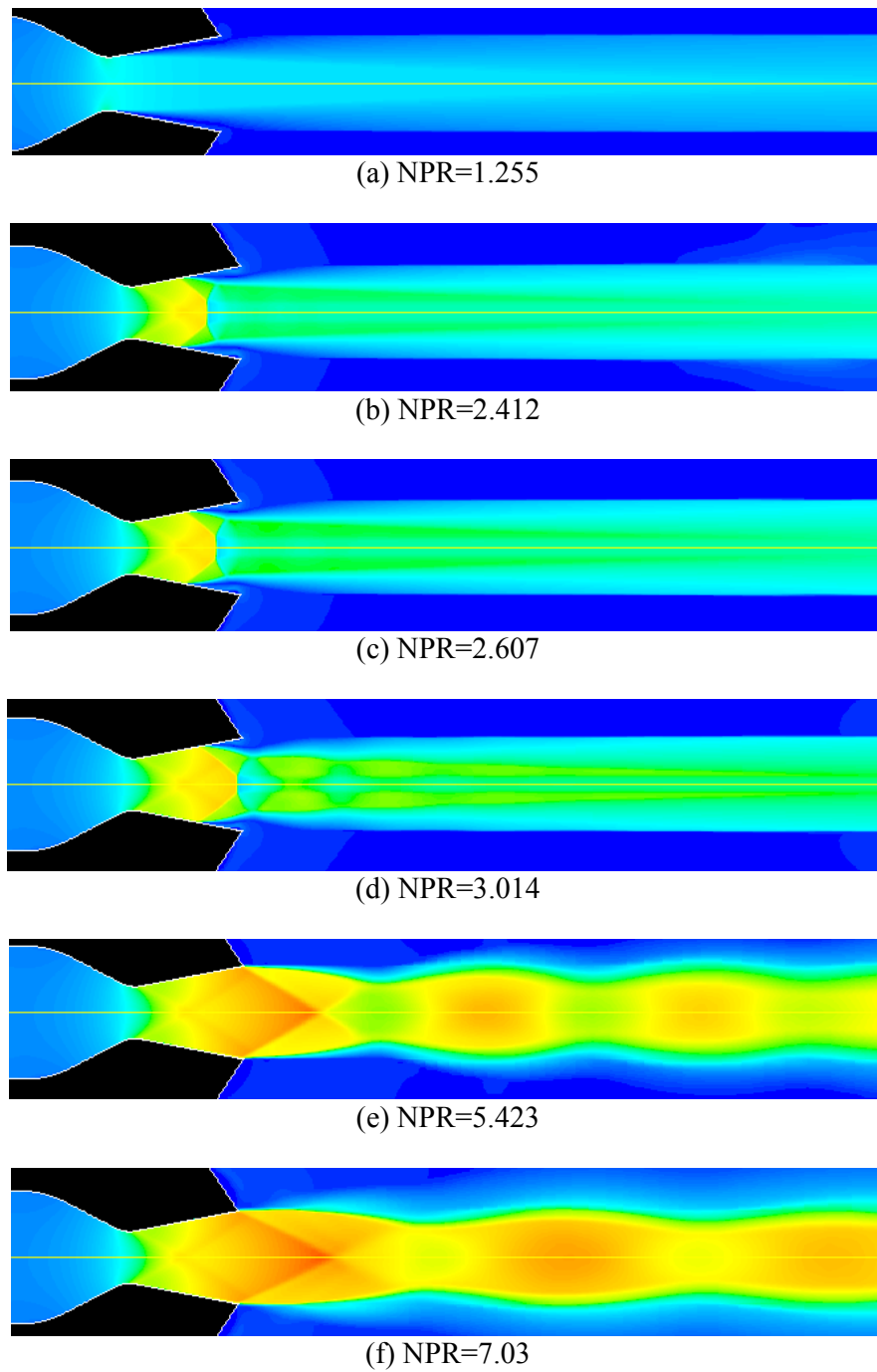


**Figure 3** The computed Mach number images for different nozzle pressure ratios

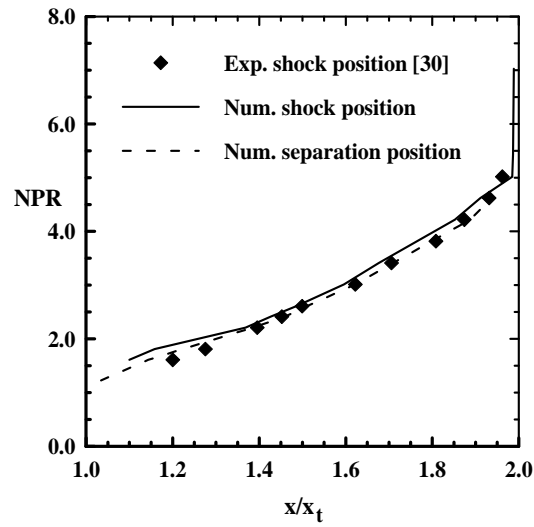


**Figure 4: Comparison of the predicted shock positions and the separation points locations**

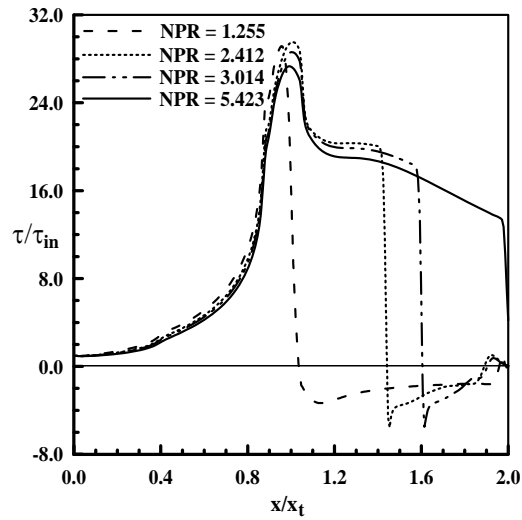


**Figure 5: The computed shear stress distribution at different NPRs**

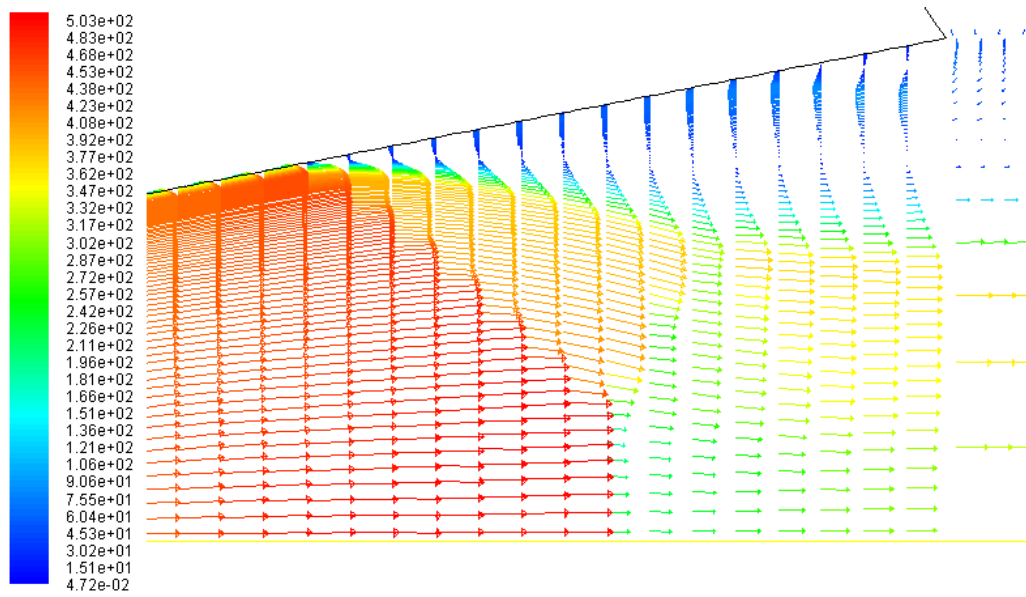


Figure 6: Velocity vector plot for NPR=2.412

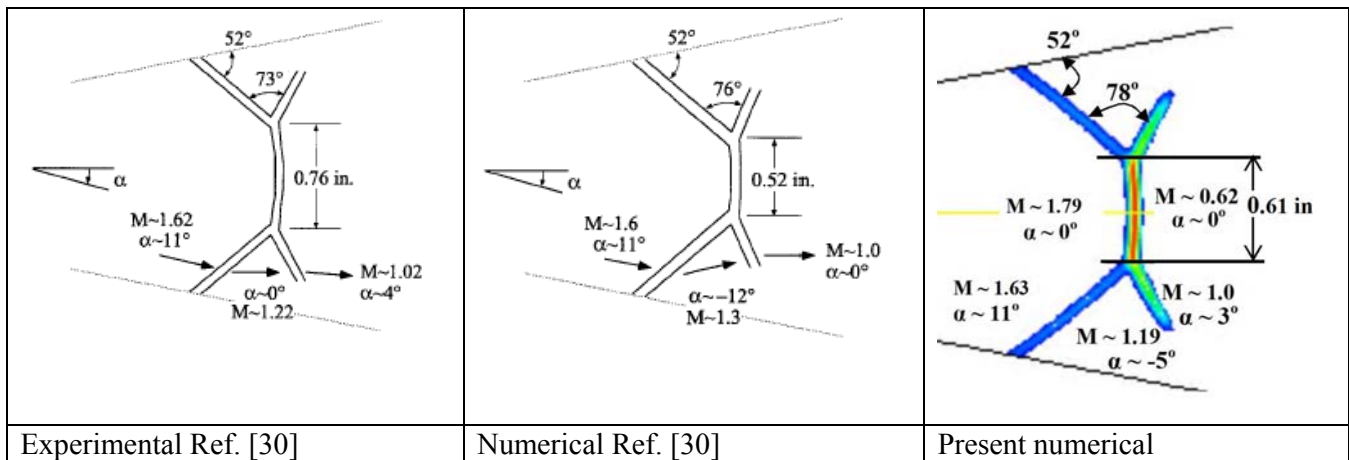


Figure 7 The comparison of the computational shock schematic, for NPR=2.412, with previous experimental and numerical results [30].

## Conclusion

The numerical simulations of compressible flow passing through a 2D solid rocket motor convergent-divergent nozzle with a fixed geometry and different nozzle pressure ratios are carried out. The predicted results are obtained by solving the RANS equations for compressible flow in its conservative form coupled with both the energy equation and the equation of a state over general curvilinear coordinates. In order to solve the governing equations, the general numerical method for heat, mass and momentum transfer proposed by Patankar 1980 is used. This numerical method is a 2-D finite volume solver based on the SIMPLE algorithm. Several turbulence models are used, namely; the standard  $k-\epsilon$  model, the extended  $k-\epsilon$  model, shear-stress transport  $k-\omega$  model, and the  $v^2-f$  model. The numerical results reveal that, the SST  $k-\omega$  model gave the best results compared with other models in

predicting the shock wave position and the separation point, while other models gave a poor prediction. The reason behind that may be related to the formulation of SST turbulence model in the gradual change from the standard  $k-\omega$  model in the inner region of the boundary layer to a high-Reynolds-number  $k-\varepsilon$  model in the outer part of the boundary layer instead of using the near-wall modeling via the wall functions. In more elaborated results, the comparison of the shock schematic with the previous numerical and experimental results show good and reasonable agreement with experimental measurements, which revealed the accuracy of the present computational methodology in predicting such phenomena.

## Acknowledgements

This work is sponsored by the Science and Technology Development Fund (STDF) through the subcontract ID-108.

## REFERENCES

- [1]. Ciucci, A., Iaccarino, G., Moser, R., Najjar, F. and Durbin, P., Simulation of rocket motor internal flows with turbulent mass injection, Science, Center for turbulence research, Proceeding of the summer program, pp. 245-266, 1998.
- [2]. Hegab, A.M. Kassoy, D.R., and Sileem, A.A. "Numerical Investigation of Acoustic-Fluid Dynamics Interaction in an SRM Chamber/Nozzle Model " AIAA Paper 98-0712, 36<sup>th</sup> Aerospace Science Meeting , Reno, NV, USA, 1998.
- [3]. Hegab, A. "Study of Acoustic Phenomena in a Solid Rocket Engines", Ph.D. Thesis, Mech. Power Engineering Dept., Menoufia Univ., Egypt, "carried out at Center for Combustion Research, University of Colorado at Boulder, USA ,1998.
- [4]. Dusa, D. J. Exhaust nozzle system design considerations for turboramjet propulsion system, Proceedings of the 10<sup>th</sup> international Symposium on Airbreathing Engines, Vol.2, AIAA, Reston, VA, pp. 1100-1110, 1991.
- [5]. Hegab A., Jackson T., Buckmaster J., Stewart D., (2001) "Nonsteady Burning of Periodic Sandwich Propellants with Complete Coupling between the Solid and Gas Phases", *Journal of Combustion and Flame*, 125, 1055-1070, 2001.
- [6]. Morrisette, E. L. and Goldberg, T.J., Turbulent flow separation criteria for overexpanded supersonic nozzles, NASA TP 1207, 1978.
- [7]. Hamed, A. and Vogiatzis, C., Overexpanded two-dimensional convergent-divergent nozzle flow simulations, Assessment of turbulence models, J. Propulsion and Power, Vol. 13, pp. 444-445, 1997.
- [8]. Hunter, C. A., Experimental, Theoretical and computational investigation of separated nozzle flows, AIAA paper, 98-3107, 1998.
- [9]. Romine, G. L., Nozzle flow separation, AIAA Journal, Vol. 36, No.9, pp. 1618-1625, 1998.
- [10]. Hamed, A. and Vogiatzis, C., Overexpanded two-dimensional convergent-divergent nozzle performance, effects of three-dimensional flow interactions, J. Propulsion and Power, Vol. 14, No. 2, pp. 234-240, 1998.
- [11]. Zill, A., Flow separation in rectangular over-expanded supersonic nozzles, 44<sup>th</sup> AIAA Aerospace Science Meeting and Exhibit, Reno Nevada, 2006.
- [12]. Johnson, A. and Papamoschou, D., Shock motion and flow instabilities in supersonic nozzle flow separation, 38<sup>th</sup> Fluid Dynamics Conference and Exhibit, Washington, 2008.
- [13]. Gikley, S. C., Hines, R. H. and Shaw, R. J., Installing a propulsion system in the HSCT, Mechanical Engineering, Vol. 117, No.8, pp.98-101, 1995.

- [14]. ElAskary, W. and Balabel, A., Prediction of reattaching turbulent shear flow in asymmetric divergent channel using linear and non-linear turbulence models, Engineering Research Journal (ERJ), Faculty of Eng., Menoufia Uni., Vol. 30, NO. 4, pp. 535-550, 2007.
- [15]. Balabel, RANS modeling of gas jet impinging onto a deformable liquid interface, Emirates Journal for Engineering Research (EJER), Vol.12(3), pp.35-46, 2007.
- [16]. Hegab, A., El-Askary, W. A., Balabel, A. and El-Behery, S., RANS simulation of turbulence in a porous channel with constant mass injection, accepted for publication in 13<sup>th</sup> international conference on Aerospace science & Aviation Technology, ASAT 2009.
- [17]. Hamed, A. and Vogiatzis, C., Assessment of turbulence models in overexpanded 2D-CD nozzles, Journal of Propulsion and Power, Vol.13, No.3, pp. 444-445, 1996.
- [18]. Hamed, A. and Vogiatzist, C., Overexpanded two-dimensional convergent-divergent nozzle performance, effects of three-dimensional flow interactions, Journal of Propulsion and Power, Vol.14, No.2, pp. 234-240, 1998.
- [19]. Hamed, A. and Vogiatzist, C., Three-dimensional flow computations and thrust predictions in 2DCD overexpanded nozzles, AIAA paper 97-0030, 1997.
- [20]. Plotkin, K.J., Shock wave oscillation driven by turbulent boundary layer fluctuations, AIAA Journal, Vol.13(8), pp. 1036-1040, 1975.
- [21]. Dussauge, J. P. Dupont, P. and debieve, J. F., Unsteadiness in Shock wave boundary layer interaction with separation, Aerospace science and Technology, Vol. 10, Issue 2, pp. 85-91, 2006.
- [22]. Bourgoing, A. and Reijasse, Ph., Experimental analysis of unsteady separated flows in a supersonic planar nozzle, shock waves, Vol.14(4), pp. 251-258, 2005.
- [23]. Patankar, S. V., Numerical Heat Transfer and Fluid Flow. McGraw Hill, New York, 1980.
- [24]. Launder, B. E. and Spalding, D. B., Mathematical models of turbulence, Academic London, pp. 169-189, 1972.
- [25]. Chen, Y. S. and Kim, S. W., Computation of turbulent flows using extended  $k-\varepsilon$  turbulence closure model, NASA CR-179204, 1987.
- [26]. Durbin, P. A., Near-wall turbulence closure modeling without damping functions, Theoretical and Computational Fluid Dynamics, Vol.3 (1), pp. 1-13, 1991.
- [27]. Menter, F. R., Two-equation eddy-viscosity turbulence models for engineering applications, AIAA journal, Vol.32(8), pp. 1598-1605, 1994.
- [28]. Launder BE, Spalding DB, The Numerical Computation of Turbulent Flows, International Journal for Numerical Methods in Fluids, Vol.15, pp. 127-146, 1974.
- [29]. Kim, S. E. and Choudhury, D., A near-wall treatment using wall functions sensitized to pressure gradient, ASME FED, Vol.217, Separated and complex flows, ASME, 1995.
- [30]. Hunter, C. A., Experimental, theoretical and computational investigation of separated nozzle flows, AIAA-98-3107, pp.1-20, 1998.
- [31]. Papamoschou, D. and Zill, A., Fundamental investigation of supersonic nozzle flow separation, AIAA paper 2004-1111, 2004.